

# Ash decline assessment in emerald ash borer-infested regions: A test of tree-level, hyperspectral technologies

Jennifer Pontius<sup>a,\*</sup>, Mary Martin<sup>b</sup>, Lucie Plourde<sup>b</sup>, Richard Hallett<sup>a</sup>

<sup>a</sup> USDA Forest Service-NRS, 271 Mast Road, Durham, NH 03024, United States

<sup>b</sup> Complex Systems Research Center, University of New Hampshire, Morse Hall, Durham, NH 03824, United States

Received 13 September 2007; received in revised form 7 December 2007; accepted 22 December 2007

## Abstract

The emerald ash borer (EAB) is an exotic insect pest currently threatening ash species in the Great Lakes region. Because of the potential impact on forests in this area, multiple government agencies are currently focusing their efforts on developing new technologies to detect, monitor and control this insect pest. Previous work has shown that hyperspectral remote sensing technologies can produce detailed maps of forest health and species abundance on a landscape scale. This study examines the capability of a commercially available sensor (SpecTIR VNIR) to map ash decline due to exotic EAB infestations in Michigan and Ohio. A 6-term linear regression equation based on known stress- and chlorophyll-sensitive indices was able to predict decline on a continuous 0- to 10 scale with an  $r$ -squared of 0.71 and an average jackknifed residual of 0.61. Treated as an integer, decline was predicted to within one class with 97% accuracy. The ability of this instrument to assess decline below class 4 (when dieback and transparency reach levels first noticeable in the field) is based upon pre-visual reductions in chlorophyll content and function that are characteristic of early stress. The identification of early stress is critical in containing newly introduced exotics such as EAB. While this decline prediction technique is not stress- or species-specific, it will enable land managers to assess and monitor detailed forest health across the landscape.

© 2008 Elsevier Inc. All rights reserved.

**Keywords:** Forest health; Pre-visual decline; *Agrilus planipennis*; EAB; Remote sensing; High resolution

## 1. Introduction

Since it was first discovered in Michigan in 2002, the emerald ash borer (EAB), *Agrilus planipennis* Fairmaire, has killed more than 15 million ash trees in Michigan, Ohio and Indiana (Maloney et al., 2006). In Ohio alone, total losses are estimated to range between \$1.8 and \$7.6 billion (Sydnor et al., 2007). If this exotic pest continues to spread across the U.S., economic impacts could reach into the hundreds of billions of dollars. Ecological impacts are also of concern due to the concentration of ash in riparian areas.

The EAB is native to Asia, where it reaches high densities on a variety of host species. In the US, EAB infestation has resulted in rapid mortality of ash of various sizes and conditions. Infestation is not easily detected in newly infested trees

(McCullough & Katovich 2004). Fine twig dieback is the primary visual symptom, followed by extensive epicormic branching in the lower portions of the trunk. As infestation progresses, significant portions of the cambium are exposed by woodpeckers feeding on EAB larvae along the bole. D-shaped exit holes and distinct S-shaped larval feeding tunnels are the most obvious direct signs of EAB (McCullough & Katovich 2004).

Currently, multiple government agencies are focusing their efforts on developing new technologies to detect, monitor and control EAB in an effort to prevent further spread. Because of the potential for rapid spread, early detection will be important for the ultimate control of this pest. One approach to early detection over large areas involves remote sensing technology. Narrow-band hyperspectral instruments have the capability to identify early signs of stress- in some cases even when symptoms are not visible to the human eye (Carter, 1993; Carter & Miller, 1994; Cibula & Carter, 1992; Mohammed

\* Corresponding author. Tel.: +1 603 868 7739; fax: +1 603 868 7604.

E-mail address: [jennifer.pontius@unh.edu](mailto:jennifer.pontius@unh.edu) (J. Pontius).

et al., 1995; Pontius et al., 2005a,b,c; Zarco-Tejada et al., 2000a, b,c). Physiologically, this can be explained by the tendency of stressed leaves to reduce photosynthetic activity and chlorophyll content. Even subtle changes in these factors can alter reflectance patterns in the visible and near-infrared (NIR) spectrum (Carter & Knapp, 2001; Gitelson & Merzlyak, 1996; Rock et al., 1988; Vogelmann & Rock, 1988; Vogelmann et al., 1993).

The use of wavelength indices or band ratios pairs stress-sensitive wavebands in combination with relatively stress-insensitive bands to correct for variation in irradiance, leaf orientation, and shading. The result is a variable that is optimized for detection of plant stress (Carter, 1994).

The majority of plant stress indices are sensitive to foliar chlorophyll content. Stress-induced changes in reflectance have been directly linked to foliar chlorophyll content in numerous studies (Gitelson & Merzlyak, 1996; Rock et al., 1988; Vogelmann et al., 1993). When plants are subjected to stress, many physiological changes occur, including: reductions in photosynthetic activity (Carter & Knapp, 2001), inhibition of chlorophyll formation (Bourque & Naylor, 1971), and an increasing breakdown of the chlorophyll molecule (Johnson, 1988). Efficient field measurements of these chlorophyll related changes have been approximated using measures of chlorophyll fluorescence (a measure of photosynthetic activity) (Strasser et al., 1995; Strasser & Tsimilli-Michael, 2001).

This paper describes techniques using commercially available hyperspectral remote sensing imagery to quantify detailed ash decline using these stress sensitive indices. Specifically our objectives were to:

1. Develop a field-based decline rating system in order to capture and summarize the range of ash decline symptoms resulting from EAB infestation.
2. Use the system developed in objective 1 to characterize ground control plots covering a range of ash abundance and health.
3. Use hyperspectral remote sensing imagery in conjunction with ground control plot data collected in objective 2 to predict ash decline over large contiguous areas.

## 2. Methods

### 2.1. Image data

Funded by a multi-agency effort to test hyperspectral technologies for forest health applications, SpecTIR flew a VNIR sensor on a fixed wing aircraft over sections of MI and OH on June 5 and 6, 2006 (Fig. 1). These regions were selected by the joint management team to cover a range of EAB infestation histories, densities and impacts. The resulting 1-m resolution imagery covers 12,000-ha with variable forest species composition and health.

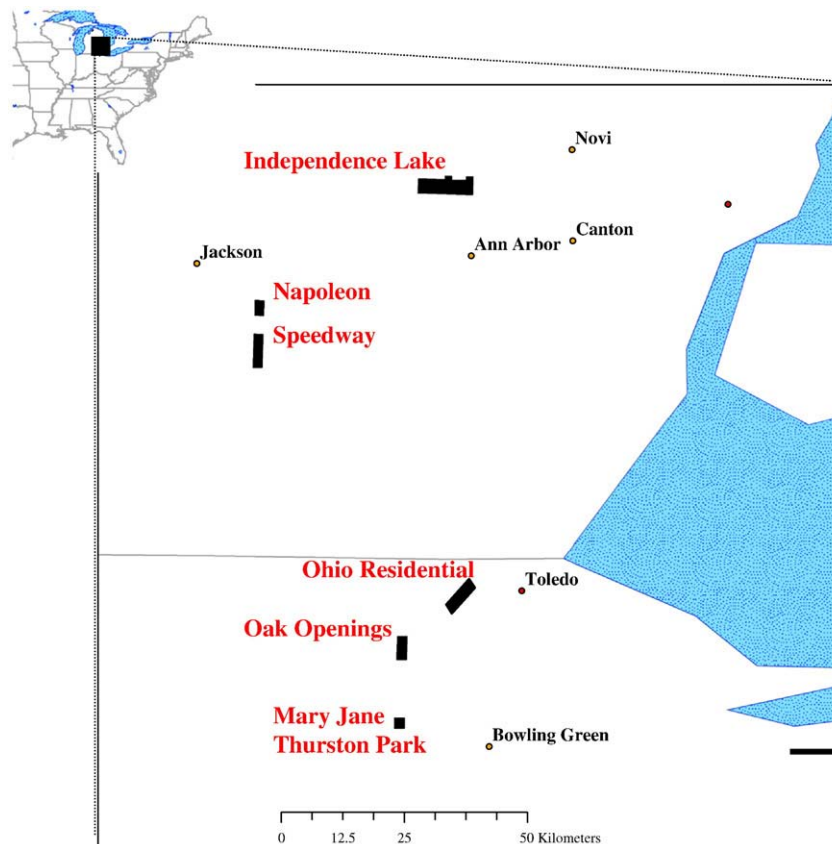


Fig. 1. Study Area. Six regions across southern MI and northern OH were flown by a SpecTIR VNIR sensor for collection of high spatial resolution hyperspectral imagery. These regions cover a range of ash density, health and EAB infestation levels.



Fig. 2. Digital Canopy Transparency. Percent canopy transparency was quantified using a digital camera zoomed in to four different locations around the canopy. A customized script converts color photographs to grayscale and then to black and white based on a user-defined threshold. Transparency is then calculated as the number of white versus total pixels. The sequence presented here is for a healthy dense canopy (a) and a thinning decline canopy (b).

SpecTIR's VNIR whiskbroom sensor has 128 6.6 nm bands with a spectral range of approximately 450 nm to 990 nm. Instrument altitude was set for a 1 m resolution collect in order to distinguish individual tree canopies in urban areas. SpecTIR delivered a Level 1 product, which included radiometrically calibrated, geometrically corrected flight lines. Other than applying the supplied INS correction to account for aircraft geometry, no additional pre-processing of the imagery was necessary. We used ENVI version 4.3 (ITT Visual Information Solutions, Boulder, Colorado) software to mask non-forested areas, extract spectra for calibration, and to predict decline on the full extent of imagery.

## 2.2. Ground truth data collection

Within a one-week window of the image data collect, we established 28 10-factor prism plots in MI and OH. The selection of these locations was based upon local knowledge of ash and EAB densities in order to maximize the range of health for prediction calibration. A stem map was created for each plot based on distance and bearing from the Trimble GPS geolocated plot center. This allowed for the calculation of sub-meter geo-location accuracy for individual tree crowns to link to the

imagery. Measurements on all trees included: species, diameter at breast height, canopy position, and crown vigor.

In addition to stem mapping data, detailed decline measurements were made on all ash species. Selecting only canopy-dominant (visible to the sensor) ash from each plot resulted in 87 canopy-dominant ash trees, of which 60 were visible in the imagery for decline equation development. The goal of assessing decline was threefold:

1. Capture the various, sequential symptoms that follow EAB infestation. While there are common stress responses in all tree species, there are also stress- and species-specific symptoms that may contain information important to decline detection. For EAB, we included several measurements commonly used in forest health assessment (vigor class, transparency, dieback and live crown ratio), measurements of early stress symptoms (chlorophyll fluorescence indices), and symptoms specific to EAB infestation (woodpecker activity, epicormic branching, and exit hole counts).
2. Create one continuous decline summary variable to link to imagery. Traditional decline assessments involve broad class variables based on one measurement like defoliation or transparency. By combining measurements from all decline

symptoms, a complete picture of stress-related canopy structure and physiology is summarized in the dependent variable. The spectral information relative to vegetation stress available with narrow-band hyperspectral sensors is not fully utilized when limited to only a few class variables for one stress symptom. Such classifications lack the precision necessary to pick up early decline symptoms or monitor small changes in health over time and limit the application of quantitative statistics.

3. Minimize subjective, ocular measurements where possible. Traditional decline assessment protocols involve subjective, ocular-based field assessments of various crown characteristics (i.e. dieback, transparency, crown vigor, and canopy density). The subjective nature of such measurements renders them vulnerable to issues of observer bias (Innes, 1998; Sucharita et al., 1995).

To this end, each canopy-dominant ash tree was tagged and sampled for a suite of decline symptoms. This included the collection of multiple sunlit branches from the upper-canopy using a 12-gauge shot gun. Measurements on sampled trees included the following variables (described in detail below): chlorophyll fluorescence measures, digital canopy transparency, digital live crown ratio, percent fine twig dieback, EAB exit hole counts, woodpecker activity and epicormic branching.

#### 2.2.1. Chlorophyll fluorescence measures

Physiologically, one of the most pronounced effects of incipient stress is a reduction in net photosynthesis (Carter & Knapp, 2001). Chlorophyll fluorescence measurements taken on dark-adapted leaves can be used to estimate overall photosynthetic capacity and photosynthetic efficiency.

To capture this early stress symptom, we measured chlorophyll fluorescence using a Handy PEA Fluorometer with a 30-minute dark adaptation time and a light intensity of 3000  $\mu\text{mol photons m}^{-2} \text{s}^{-1}$ . We used the Handy PEA software to calculate Performance Index (PI) and FvFm values following the O–J–I–P test described in Strasser et al. (1995) on five sun leaves from various portions of the upper canopy. We then used the average PI and FvFm value from each subject tree in the final health calculations.

#### 2.2.2. Transparency

Digital photographs from multiple locations around the tree were used to quantify crown transparency. The benefit of this technique is the direct, mathematical quantification of transparency that can detect minute differences in canopy transparency, while minimizing user bias.

Four different digital photos were taken from around the subject canopy. We used a 10 $\times$  optical zoom to ensure that all photographs excluded the main bole and the sky outside the perimeter of the main canopy. We normalized varying light conditions using automatic shutter speed and aperture settings.

We wrote a custom script to extract percent transparency from digital photographs. The first step transforms color photos to a 1–255 grayscale image. Through visual examination of all photos, we determined that a threshold value of 180 was the

most robust value to convert grayscale images to accurate black and white binary files. Percent transparency was then calculated based on the number of light pixels as a percentage of all pixels in the image. The program also generates a composite image of the original, gray scale, and black and white photos for a visual quality check of correct classification of light (sky) and dark (foliage) pixels (Fig. 2). An access database was then utilized to average output from the four photos of each subject tree to determine a final transparency value.

#### 2.2.3. Percent fine twig dieback

The percent fine twig dieback measure considers dead branches <2.5 cm diameter with mortality beginning at the terminal portion of the limb and progressing inward. Following FIA guidelines (USDA Forest Service 1997), two observers classified dieback to the nearest 5% class after examining the entire canopy of each subject tree.

#### 2.2.4. Live crown ratio

One of the final and most obvious symptoms of severe decline is a gradual reduction in the size of the photosynthetically active canopy. Live crown ratio is calculated by measuring the size of the live crown (total tree height minus the base of the live crown) divided by the total tree height. The base of the live crown is defined as the lowest live foliage that is on a branch at least 2.5 cm in diameter and within 1.5 m of the next live branch (USDA Forest Service, 2004).

#### 2.2.5. Crown vigor rating

The crown vigor rating is based on an ocular assessment of the overall crown condition. Assigned values range from 1 to 5 and were estimated according to Millers et al. (1991):

- 1 = healthy (no major branch mortality)
- 2 = light decline (10 to 25% of crown damaged)
- 3 = moderate decline (26 to 50% of crown damaged)
- 4 = severe decline (>50% of crown damaged)
- 5 = dead

#### 2.2.6. Infestation symptoms

In addition to some of the more commonly used methods of rating tree health, we included variables designed to quantify some of the symptoms of EAB infestation and the specific stress responses elicited by ash trees. These included epicormic branching, woodpecker damage, and EAB exit holes. Similar to crown vigor, epicormic branching and woodpecker activity were divided up into 5-class categories. Epicormic branching included any shoots or leaves sprouting from the main bole. Woodpecker activity was witnessed as white patches on the main bole where the outer bark had been peeled away. The entire main bole was included in estimating the proportion impacted. Classes were assigned as 0 = no evidence, 1 = trace to 10%, 2 = 11% to 25%, 3 = 26% to 50%, 4 = 51% to 75%, and 5 = greater than 75% of the bole impacted. Exit holes from larvae are the most obvious, direct evidence of EAB infestation. We examined the main bole of each subject tree from 0.5 to 1.5 m above the ground, counting every D-shaped hole as an estimate of EAB activity.

2.2.7. Summary decline rating calculation

In order to calibrate the spectral response of the canopy and create an equation that could be used to predict tree health, we created a single decline rating variable which normalizes and integrates all of the individual health measures described above.

The first step in accomplishing this task was to normalize each individual health variable to the same scale. Using JMP Start statistical software, a 10-class quantile distribution analysis was conducted on each variable in order to determine the appropriate thresholds for class assignments. We used these thresholds to translate the raw data to a 0–10 classification, where 0 represents a perfectly healthy tree and a value of 10 means the tree is dead (Table 1).

Example output from a quantile analysis in Table 2 shows clear thresholds for continuous variables such as percent transparency. Categorical variables tend to be more confusing. In such cases, each measured class value is assigned the average normalized value (Table 3). This retains the original number of categories while normalizing them to a 0 to 10 scale.

Tables 4 and 5 describe the assigned class thresholds that we used to normalize all measured variables to the 0 to 10 scale. These assignments were made based on the quantile distribution of values from 87 ash trees sampled as a part of study. We then averaged the normalized values to produce one overall continuous decline value (Table 6). This final decline value represents a synthesis value of all measured decline variables.

2.3. Equation development

We calculated wavelengths and indices related to plant stress (Table 7) from the spectra extracted from the imagery for each subject tree. These were entered into a mixed-stepwise linear regression to identify the strongest set of predictor variables. For an *N* of 60 trees, we limited the final equation to a maximum of 6 terms and set limits to enter at 0.05 and to leave at 0.01 to avoid overfitting the equation (Williams & Norris 2001). The mixed platform tests all possible linear regression combinations and reports the set producing the lowest standard error of calibration. Variables are entered in the order of greatest significance and retained only if they remain significant as

Table 1  
Field-measurement normalization by quantiles (continuous variables)

Quantile	Measured % transparency	Class assignment
100% max possible value (dead)	100.0	10
99.50%	41.1	9
97.50%	37.9	8
90.00%	31.4	7
75.00%	26.7	6
50% median measured value	20.6	5
25.00%	14.9	4
10.00%	10.5	3
2.50%	9.0	2
0.50%	8.4	1
0% min possible value	0.0	0

Ten-class quantiles were used to establish cut-offs in translated field-measured values to a normalized, 10-class scale. Here are the calculated quantiles for percent transparency based on the 87 ash trees measured in this study.

Table 2  
Field-measurement normalization by quantiles (categorical variables)

Quantile	Measured crown vigor	Class assignment
100% max possible value	5	10
99.50%	5	9
97.50%	4	8
90.00%	4	7.5
75.00%	3	
50% median measured value	3	5.5
25.00%	2	
10.00%	1	3
2.50%	1	2
0.50%	1	
0% min possible value	0	0

Quantile-derived cut-offs for field-measured categorical variables were not as straightforward to normalize. Here, we use crown vigor as an example of how measured classes were assigned the average normalized class assignment.

additional variables are added. In order to limit autocorrelation, variables were retained in the final model only if the variance inflation factor was below ten (Kleinbaum et al., 1998). Jackknifed residuals calculated from the PRESS statistic were used to assess the stability of the final predictive equation as a measure of independent validation accuracy (Kozak & Kozak 2003).

We applied the final decline model to the imagery on a pixel-by-pixel basis using the Band Math function in ENVI. Non-forested areas were identified with a supervised classification (Spectral Angle Mapper) and masked in ENVI to ensure equation application to forested areas only.

3. Results and discussion

3.1. Ground truth data

From the 28 plots in MI and OH, we sampled 60 canopy-dominant ash trees with crowns clearly visible to the airborne sensor. Diameter at breast height varied from 11 cm in a very young stand, to 95.8 cm in a mature stand. The final decline rating ranged from 2.07 (healthy) to 10 (dead) (Table 7). Decline was significantly higher ( $p=0.0012$ ) in the MI stands (average decline=4.9 at Independence Lake and 4.2 at Speedway) where EAB infestation was identified in the late 1990s. The uninfested southern OH stand was the healthiest (average decline=2.8 at Mary Jane Thurston State Park), while the ash trees in the northern OH stand were beginning to show early signs of decline (Oak Openings State Park=3.9). Incipient EAB infestation was confirmed by the presence of several exit holes on six of the trees sampled at Oak Openings.

Specific signs of EAB infestation are typically not evident until the tree is showing other signs of physiological stress. This is illustrated in Fig. 3 where we see no evidence of epicormic branching on any trees below an overall decline class of 3, no woodpecker activity on any trees with an overall decline class less than 4, and minimal numbers of exit holes on trees below an

Table 3  
Quantile cut-offs (continuous variables)

Field measured values						
Class assignment for averaging	Percent dieback	Percent live crown	Percent digital canopy transparency	FvFm	Performance index (PI)	EAB exit hole count
0	0	93 to 100	<2	0.8498 to 0.850	>10	0
1		88 to 92	2 to 8	0.8491 to 0.8497	6.15 to 10	1 to 2
2	5	75 to 87	9 to 11	0.8477 to 0.8490	6.10 to 6.14	3 to 5
3		67 to 74	12 to 15	0.842 to 0.8476	5.18 to 6.09	6 to 8
4	10	58 to 66	16 to 21	0.836 to 0.841	4.41 to 5.17	9 to 19
5	15	48 to 57	22 to 28	0.825 to 0.835	3.42 to 4.40	20 to 30
6	20	34 to 48	29 to 33	0.813 to 0.824	2.71 to 3.41	30 to 50
7	25 to 40	23 to 34	34 to 37	0.749 to 0.812	1.99 to 2.70	51 to 84
8	45 to 85	11 to 23	38 to 41	0.733 to 0.748	1.46 to 1.98	85 to 119
9	90 to 95	1 to 10	42 to 71	0.999 to 0.732	1.32 to 1.45	120 to 128
10	100	0	72 to 100	0 to 0.1	0 to 1.31	>128

Quantile cut-off values to normalize measurements to a 0–10 scale were calculated from the 87 ash sampled in Michigan and Ohio. Measurements were assigned a class value based on these cut-offs and then averaged to produce one summary decline rating.

overall decline class of 5. This indicates that EAB infestation is not visibly detectable until infestation has already affected tree health. This suggests that visible signs of infestation such as exit hole counts, epicormic branching, or woodpecker damage are not reliable for detecting incipient EAB infestation.

3.2. Decline predictions

While multiple indices were significantly correlated ( $p < 0.01$ ) with decline (Table 6), the stepwise multiple linear regression was limited to 6 terms to avoid overfitting. The final, best-fit model included primarily chlorophyll and canopy water content sensitive indices (Table 8, Fig. 5). Validation of the continuous decline prediction resulted in an r-square of 0.71 and RMSE of 0.582 (Fig. 4). An average jackknifed residual error (0.61 compared to RMSE=0.58) indicates that we could expect this model to perform similarly on an independent data set. When the continuous decline rating is rounded to the nearest integer for class comparison, the model was able to predict decline for the calibration data with 63% accuracy and an accuracy of 97% to within one class.

3.3. Key variables

The most heavily weighted variable retained in the regression model was the chlorophyll<sub>a</sub> sensitive CSc index identified by

Table 4  
Quantile cut-offs (categorical variables)

Field measured class	Class assignment value		
	Crown vigor	Epicormic rating	Woodpecker activity
0	0	0	0
1	2	1.5	3
2	4	4	6
3	5.5	6	8
4	7.5	8	9
5	10	9.5	10

Class assignments for categorical variables were averaged by quantile to match the original number of groupings.

Carter and Miller (1994) as a measure of early stress detection in soybeans (scaled estimate=2.71). CSc is calculated as the ratio of reflectance at R<sub>605</sub> / R<sub>760</sub>. Carter (1994) found that this index responded consistently and significantly to eight different stress agents across 6 different plant species in laboratory studies. The significance of this index results from the weak absorbance of chlorophyll at 605 nm where small decreases in chlorophyll content result in significant increases in leaf reflectance.

The second most heavily weighted variable in our model was Gmb (scaled estimate=2.52). Developed by Gitelson and Merzlyak (1994), this ratio of reflectance at R<sub>750</sub> / R<sub>700</sub>, was found to be directly proportional to chlorophyll concentration of sugar maple and horse chestnut leaves collected at various intervals over the growing season. Additional studies determined that Gmb is accurate for assessing chlorophyll content at both the leaf and canopy levels (Gitelson et al., 1996) and for direct estimation of early stages of plant stress (Carter, 1993, 1994).

A third chlorophyll sensitive wavelength (scaled estimate=−0.91) retained in our model was the ratio of first derivative spectra at FD<sub>715</sub> / FD<sub>705</sub> (Vogb). Laboratory measurements found that this parameter was highly correlated with variation in total chlorophyll content in sugar maple experiencing various levels of insect damage (Vogelmann et al., 1993). This index is

Table 5  
Example decline rating calculation

Variable	Measured value	Class assignment
Crown vigor	4	7.5
Dieback	80	7
Epicormic rating	1	1.5
Exit hole count	30	5
FvFm	0.84	4
Live crown ratio	0.54	5
PI	3.40	5
Transparency	29.82	6
Woodpecker rating	2	6
Average		5.22

A sample calculation of overall decline rating shows the field-measured value for each variable, its normalized class assignment and the final average value to be used in equation development.

Table 6  
Plant stress sensitive spectral indices

Variable	Formula	Citation	Correlation	Signif prob
Achl	$R_{550}/R_{800}$	Aoki, Yabuki, and Totsuka (1981)	0.62	0.00
Bna	$R_{800} - R_{550}$	Buschman and Nagel (1993)	-0.42	0.00
BNb	$R_{800}/R_{550}$	Buschman and Nagel (1993)	-0.59	0.00
<b>CSc</b>	<b><math>R_{605}/R_{760}</math></b>	<b>Carter (1994)</b>	<b>0.64</b>	<b>0.00</b>
CSd	$R_{710}/R_{760}$	Carter (1994)	0.57	0.00
Cse	$R_{695}/R_{760}$	Carter (1994)	0.60	0.00
Datt c	$FD_{754}/FD_{704}$	Datt (1999)	-0.44	0.00
DVI	$R_{800} - R_{680}$	Tucker (1979)	-0.38	0.00
EZ	Sum FD 625 to 795	Elvidge and Zhikang (1995)	-0.39	0.00
FD 717	FD 717	Pontius et al. 2005	-0.28	0.03
FD720	FS720	Boochs et al. (1990)	-0.34	0.01
Flo	$FD_{690}/FD_{735}$	Mohammed et al. (1995)	0.52	0.00
FP	Sum FD 680 to 780	Filella and Penuelas (1994)	-0.38	0.00
<b>GI</b>	<b><math>R_{554}/R_{677}</math></b>	<b>Smith et al. (1995)</b>	<b>-0.04</b>	<b>0.78</b>
GM	$R_{750}/R_{550}$	Gitelson and Merzlyak (1994)	-0.60	0.00
<b>Gmb</b>	<b><math>R_{750}/R_{700}</math></b>	<b>Gitelson and Merzlyak (1994)</b>	<b>-0.48</b>	<b>0.00</b>
Mac	$(R_{780} - R_{710}) / (R_{780} - R_{680})$	Maccioni et al 2001	-0.40	0.00
McM	$R_{700}/R_{760}$	McMurtey et al 1994	0.59	0.00
mND705	$(R_{750} - R_{705}) / (R_{750} + RR_{705} + 2R_{445})$	Sims and Gamon (2002)	-0.56	0.00
MSR705	$(R_{750} - R_{445}) / (R_{705} - R_{445})$	Sims and Gamon (2002)	-0.49	0.00
NDI	$(R_{750} - R_{705}) / R_{750} + R_{705}$	Gitelson and Merzlyak (1994)	-0.49	0.00
NDVI	$(R_{800} - R_{680}) / (R_{800} + R_{680})$	Gamon et al., (1997)	-0.53	0.00
<b>NPQI</b>	<b><math>(R_{415} - R_{435}) / (R_{415} + R_{435})</math></b>	<b>Barnes (1992)</b>	<b>-0.41</b>	<b>0.00</b>
OSAVI	$(R_{800} - R_{680}) / (R_{800} + R_{680} + 0.16)$	Rondeaux et al., (1996)	-0.53	0.00
PSNDb	$(R_{800} - R_{635}) / (R_{800} + R_{635})$	Blackburn (1998)	-0.58	0.00
PSSRb	$R_{800}/R_{635}$	Blackburn (1998)	-0.55	0.00
R 950	R 950	Williams and Norris (2001)	-0.38	0.00
R760	$R_{760}$	Carter and Miller (1994)	-0.38	0.00
R800	$R_{800}$	Osborne and Fearn (1986)	-0.36	0.00
RDVI	$\text{sqrt}(\text{NDVI} * \text{DVI})$	Roujean and Breon (1995)	-0.43	0.00
REIP	FD max near 700	Gitelson et al. (1996); Vogelmann et al. (1993)	-0.31	0.02
RVI	$R_{800}/R_{680}$	Pearson and Miller (1972)	-0.51	0.00
SD707	SD707	Pontius et al. (2005)	-0.57	0.00
TVI	$0.5 * (120 * (\text{Ravg}760\text{to}800 - \text{Ravg}530\text{to}570) - (200 * (\text{Ravg}650\text{to}680 - \text{Ravg}530\text{to}570)))$	Broge and Leblanc, (2001)	-0.31	0.02
Voga	$R_{740}/R_{720}$	Vogelmann et al. (1993)	-0.46	0.00
<b>Vogb</b>	<b><math>FD_{715}/FD_{705}</math></b>	<b>Vogelmann et al. (1993)</b>	<b>-0.05</b>	<b>0.69</b>
<b>WBI</b>	<b><math>R_{970}/R_{900}</math></b>	<b>Carter (1993)</b>	<b>0.57</b>	<b>0.00</b>

Existing plant stress indices were calculated from the spectra of each sample pixel. While all of these were significantly correlated with ash decline, only six (bold) were retained in the final decline predictive equation.

not sensitive to differences in green leaf biomass or background condition, which is important for remote sensing studies where canopy characteristics vary widely from pixel to pixel (Vogelmann et al., 1993).

The Normalized Phaeophytinization Index (NPQI) calculated as  $(R_{415} - R_{435}) / (R_{415} + R_{435})$  was also retained in the predictive model (scaled estimate=-0.61). NPQI is an expression of the ratio of chlorophyll<sub>a</sub> to phaeophytin<sub>a</sub> content in the leaf and reflects a relative measure of the degree of chlorophyll

degradation (Barnes, 1992). Penuelas et al. (1995) linked NPQI directly to mite-induced stress at the leaf level. It has also been shown as a strong detector of early stress in bark beetle-damaged lodgepole pine (Ahern, 1988; Lorenzen & Jensen, 1989).

The greenness index (GI) (scaled estimate=1.03) is one of the classic vegetation indices that quantifies the essential “greenness” contained within a given pixel. It has been most strongly linked to leaf area index and other structural stand characteristics as opposed to leaf pigment concentration.

Table 7  
Decline data distribution

	dbh	Decline	PI	FvFm	Transp.	Dieback	Live crown	Crown vigor	Epicormic rating	Exit hole count	Woodpecker rating
Avg	39.8	4.0	2.8	0.6	20.1	26.8	0.6	2.6	1.3	7.8	1.4
Min	11.4	2.1	0.0	0.0	0.0	0.0	0.0	1.0	0.0	0.0	0.0
Max	95.8	10.0	6.2	0.8	41.1	90.0	0.9	5.0	5.0	125.0	4.0
Stdev	16.7	1.3	1.8	0.4	8.4	23.8	0.2	1.0	0.9	19.6	0.8

The 87 trees sampled for this study covered a range of size class, health, and EAB infestation densities.

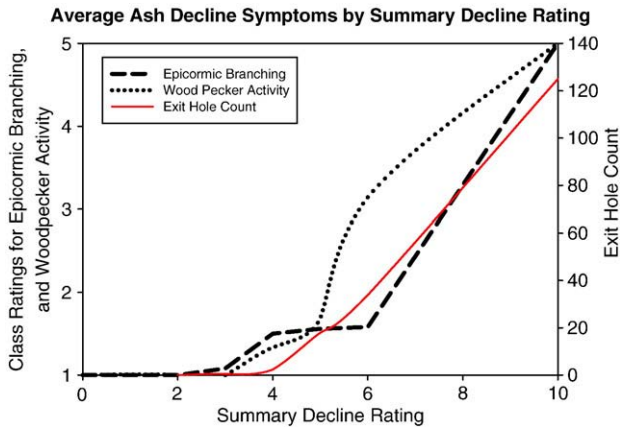


Fig. 3. EAB Infestation Symptoms. Direct signs of EAB are not typically witnessed until decline class 3 or 4, well after stress-induced changes in chlorophyll content and function.

However, more recent studies have shown a significant relationship between GI and chlorophyll<sub>a&b</sub> concentrations (Zarco-Tejada et al., 2005; Zarco-Tejada et al., 2000b; Zarco-Tejada et al., 2001). It is expected that the GI would have a lower sensitivity to early plant stress (Zarco-Tejada, 2000). Instead, it primarily serves as an indicator of prolonged vegetation stress resulting from changes in canopy structure (Zarco-Tejada, 2000). This index is probably most useful in detecting stands in more advanced stages of decline.

The Water Band Ratio (WBI) is a ratio between the reflectance at R<sub>970</sub>, where absorbance by water is evident, and R<sub>900</sub> used as a reference, or “control” band. Several studies have shown that the WBI is sensitive to changes in leaf relative water content, leaf water potential and stomatal conductance (Bull, 1991; Penuelas et al., 1993; Penuelas et al., 1996; Penuelas et al., 1994). In some species, WBI is able to detect even mild water stress (Penuelas

Table 8  
Final predictive decline equation

Variable	Index formula	Parameter estimate	Association	Reference
Intercept		-18.859		
CSc	R605/R760	53.041	Chlorophyll <sub>a</sub>	Carter (1994)
GI	R554/R677	1.868	Leaf area index, chlorophyll <sub>ab</sub>	Smith et al. (1995)
Vogb	FD715/FD705	-2.952	Total chlorophyll content	Vogelman et al. (1993)
NPQI	(R415 - R435) / (R415 + R435)	-10.77	Chlorophyll degradation	Barnes et al., (1992)
GMb	R750/R700	1.683	Total chlorophyll content	Gitelson and Merzlyak (1994)
WBI	R970/R900	7.002	Canopy water content	Carter (1993); Penuelas et al., 1997; Tucker 1980

The six indices retained in the final decline predictive equation are known to be sensitive to plant stress according to various field and laboratory studies. These indices were comprised primarily of chlorophyll-sensitive wavelengths, which correspond to the expected reduction in chlorophyll content and photosynthetic function in stressed leaves.

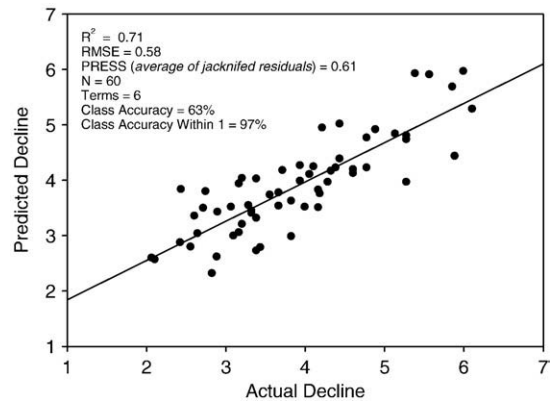


Fig. 4. Validation Results. A six-term linear regression model based on chlorophyll and water sensitive indices was able to predict a detailed 10-class decline rating for ash with a one-class tolerance accuracy of 97%.

et al., 1996). Its inclusion in the predictive model is likely due to the disruption of water transport from EAB larvae feeding in the cambial region resulting in foliar desiccation.

### 3.4. Image products

The final equation was applied to the imagery on a pixel-by-pixel basis, resulting in a decline rating for all forested pixels. More severe decline (average decline=2.9) is evident in the forested stands of southeastern Michigan (Fig. 6). This coincides with the longest known EAB infestation. By comparison, the southernmost study areas located in OH were not infested with EAB at the time the imagery was collected and have an average decline rating of 0.9 (Fig. 7). The northernmost study area in Ohio shows higher average decline ratings (average decline=2.7) indicating the possibility of incipient EAB infestation (Fig. 8). This highlights an area where management agencies might focus their ground efforts to locate newer infestations.

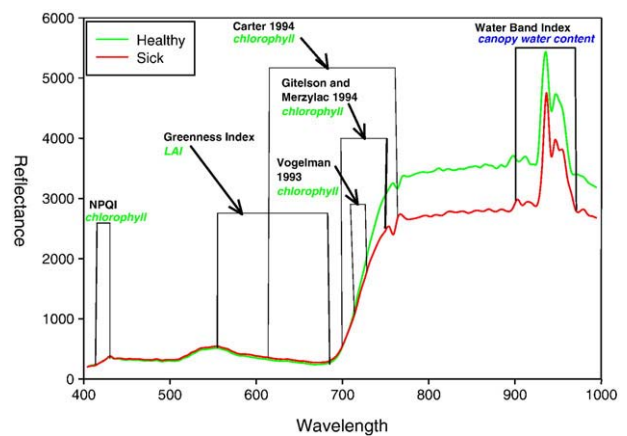


Fig. 5. Key Wavelengths. The full visible and NIR spectrum are not required to predict ash decline. Here we used 6 known plant stress indices which are sensitive to changes in chlorophyll content, function or canopy water content. Such indices generally pair a stress sensitive wavelength, with an insensitive wavelength in order to account for differences in shading, view angle or background interferences.

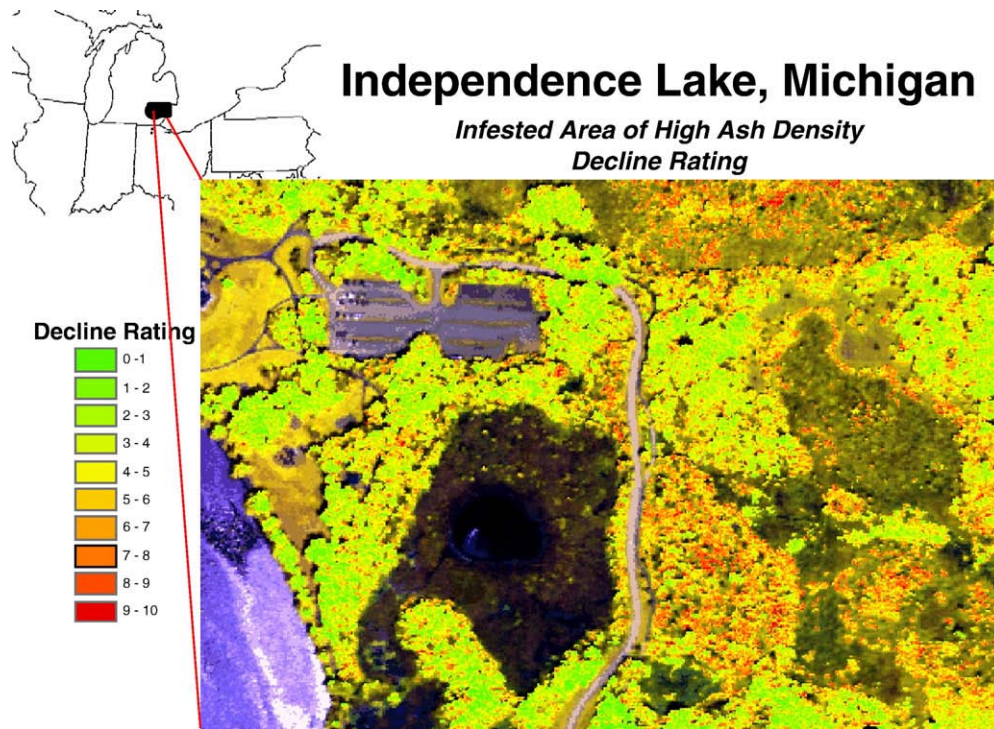


Fig. 6. Decline Close-Up: Independence Lake, MI. The predicted decline coverage over Independence Lake, a region of high ash density and prolonged EAB infestation, highlights large areas of high decline. Average forest decline was 4.9 on the 0 to 10 scale.

Plant-physiological responses to stress are similar regardless of the cause of stress (Chapin, 1991). Therefore, we can not conclude that declining trees identified in our coverages are infested with EAB. However, detection of incipient infestations can be facilitated by identifying areas of low-level decline for concentrated ground team inspection.

#### 4. Conclusions

The field-based decline rating system developed for this study was able to capture and summarize the full range of ash decline that existed within the study areas. These data were used in conjunction with hyperspectral remote sensing imagery to

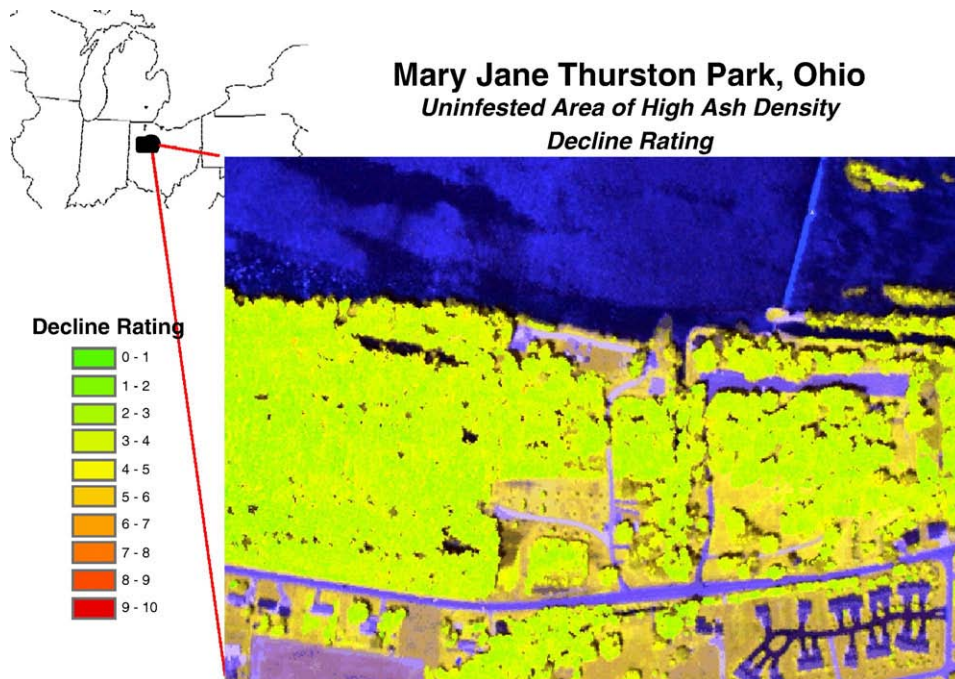


Fig. 7. Decline Close-Up: Mary Jane Thurston Park, OH. The predicted decline coverage over Mary Jane Thurston Park, a region of high ash density and no known EAB infestation, shows an abundantly healthy forest. Average decline was 2.1 on the 0 to 10 scale.

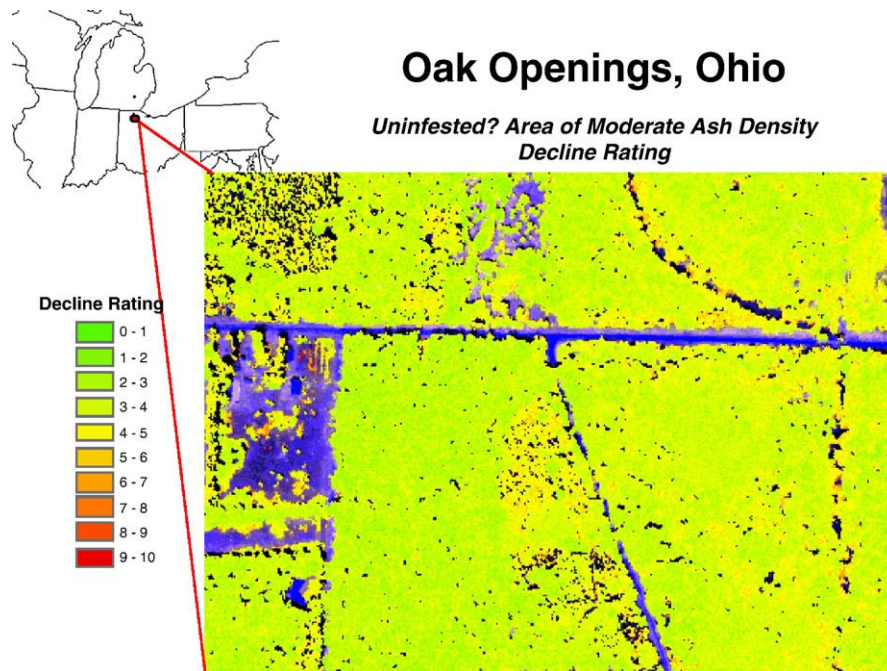


Fig. 8. Decline Close-Up: Oak Openings, OH. Oak Openings lies in northern OH where EAB infestation has not yet been reported. However, the predicted decline coverage of the region does show several areas of declining tree health. These are concentrated along riparian areas where ash is a common component. Average decline was 3.9 on the 0 to 10 scale, indicating that ground crews may wish to target this area for ground surveys of EAB spread.

create continuous coverages of predicted forest health with an emphasis on ash species in areas that are currently being impacted by EAB infestation.

This study shows that commercially available airborne hyperspectral imagery can be used to produce detailed ash decline maps for relatively large areas. Seventy one percent of the variability in ash decline was accounted for with 6 chlorophyll- and canopy water content-sensitive indices. Given that this predictive equation holds at the low end of our continuous decline rating scale, before decline symptoms are visible to observers on the ground, these techniques could be particularly valuable to land managers that need to direct field crews to areas of possible incipient infestation to identify problems early.

Compared to traditional decline classification, this hyperspectral based predictive model differentiated 5 decline classes with 97% accuracy. This represents an improvement in both accuracy and detail over more common multi-spectral remote sensing assessments of forest health. However, the extent to which these techniques can be used to monitor forest health is still unclear due to high costs, limited availability, and complex processing requirements. We anticipate that over time, competition in the private sector and currently planned satellite sensors will make this technology available to a wider audience.

The combination of traditional plot-level forest health assessment techniques with commercially available hyperspectral remote sensing imagery presented here can produce accurate, detailed, large scale maps of forest health. These data products, which can highlight areas of pre-visual tree decline, represent a significant advance in our ability to identify forest health problems earlier than ever. Utilizing these capabilities is essential to

the ultimate identification, containment and control of current and future invasive pests.

### Acknowledgements

The authors gratefully acknowledge the U.S. Forest Service Forest Health Technology Enterprise Team and the USDA Animal and Plant Health Inspection Service for allowing us to utilize the SpecTIR imagery. Funding for field work and image calibration was provided by U.S. Forest Service Eastern Forest Environmental Threat Assessment Center, with logistical support provided by the APHIS Lab in Brighton, MI, Independence Lake State Park and Ohio Metro Parks. We specifically would like to thank Dennis Souto and Danny Lee for their support through the development of this and similar applications.

### References

- Ahern, F. J. (1988). The effects of bark beetle stress on the foliar spectral reflectance of lodgepole pine. *International Journal of Remote Sensing*, 9, 1451–1468.
- Aoki, M., Yabuki, K., & Totsuka, T. (1981). An evaluation of chlorophyll content of leaves based on the spectral reflectivity in several plants. *Research Report of the National Institute of Environmental Studies of Japan*, 66, 125–130.
- Barnes, J. D. (1992). A reappraisal of the use of DMSO for the extraction and determination of chlorophylls a and b in lichens and higher plants. *Environmental Experimental Botany*, 2, 85–100.
- Blackburn, G. A. (1998). Quantifying Chlorophylls and Carotenoids at Leaf and Canopy Scales: an Evaluation of Some Hyperspectral Approaches. *Remote Sensing of Environment*, 66, 273–285.
- Boochs, F., Kupfer, G., Dockter, K., & Kuhbauch, W. (1990). Shape of the red edge as vitality indicator for plants. *International Journal of Remote Sensing*, 11(10), 1741–1753.

- Bourque, D. P., & Naylor, A. W. (1971). Large effects of small water deficits on chlorophyll accumulation and ribonucleic acid synthesis in etiolated leaves of jack bean (*Canavalia ensiformis* (L.) D.C.). *Plant Physiology*, 47, 591–594.
- Broge, N. H., & Leblanc, E. (2001). Comparing Prediction Power and Stability of Broadband and Hyperspectral Vegetation Indices for Estimation of Green Leaf Area Index and Canopy Chlorophyll Density. *Remote Sensing of Environment*, 76, 156–172.
- Bull, C. R. (1991). Wavelength selection for near-infrared reflectance moisture meters. *Journal of Agricultural Engineering Research*, 49, 113–125.
- Buschman, C., & Nagel, E. (1993). *In vivo* spectroscopy and internal optics of leaves as a basis for remote sensing of vegetation. *International Journal of Remote Sensing*, 14, 711–722.
- Carter, G. A. (1993). Responses of leaf spectral reflectance to plant stress. *American Journal of Botany*, 80, 239–243.
- Carter, G. A. (1994). Ratios of leaf reflectances in narrow wavebands as indicators of plant stress. *International Journal of Remote Sensing*, 15, 697–703.
- Carter, G. A., & Knapp, A. K. (2001). Leaf optical properties in higher plants: Linking spectral characteristics to stress and chlorophyll concentration. *American Journal of Botany*, 88, 677–684.
- Carter, G. A., & Miller, R. L. (1994). Early detection of plant stress by digital imaging within narrow stress-sensitive wavebands. *Remote Sensing of Environment*, 50, 295–302.
- Chapin, F. S. (1991). Integrated responses of plants to stress. *Bioscience*, 41, 29–36.
- Cibula, W. G., & Carter, G. A. (1992). Identification of a far red reflectance response to ectomycorrhizae in slash pine. *International Journal of Remote Sensing*, 13, 925–932.
- Datt, B. (1999). Visible/near infrared reflectance and chlorophyll content in Eucalyptus leaves. *International Journal of Remote Sensing*, 20(14), 2741–2759.
- Elvidge, C. D., & Chen, Z. (1995). Comparison of broad-band and narrow band red and near-infrared vegetation indices. *Remote Sensing of Environment*, 54, 38–48.
- Filella, I., & Penuelas, J. (1994). The red edge position and shape as indicators of plant chlorophyll content, biomass, and hydric status. *International Journal of Remote Sensing*, 15, 1459–1470.
- Gamon, J. A., Serrano, L., & Surfus, J. S. (1997). The photochemical reflectance index: an optical indicator of photosynthetic radiation use efficiency across species, functional types, and nutrient levels. *Oecologia*, 112, 492–501.
- Gitelson, A. A., & Merzlyak, M. N. (1994). Quantitative estimation of chlorophyll-a using reflectance spectra: Experiments with autumn chestnut and maple leaves. *Journal of Photochemical Phytobiology*, 22, 247–252.
- Gitelson, A. A., & Merzlyak, M. N. (1996). Signature analysis of leaf reflectance spectra: algorithm development of remote sensing of chlorophyll. *Journal of Plant Physiology*, 148, 494–500.
- Gitelson, A. A., Merzlyak, M. N., & Lichtenthaler, H. K. (1996). Detection of Red Edge Position and Chlorophyll Content by Reflectance Measurements Near 700 Nm. *Journal of Plant Physiology*, 148, 501–508.
- Innes, J. L. (1998). An assessment of the use of crown structure for the determination of the health of beech (*Fagus sylvatica*). *Forestry*, 71(2), 113–130.
- Johnson, J. D. (1988). Stress physiology of forest trees: The role of plant growth regulators. *Plant Growth Regulation* (pp. 193–215). Dordrecht: Martinus Nijhoff Publishers.
- Kleinbaum, D. G., Kupper, L. L., Muller, K. E., & Nizam, A. ((1998)). *Applied Regression Analysis and Other Multivariable Methods*. New York: Duxbury Press.
- Kozak, A., & Kozak, R. (2003). Does cross validation provide additional information in the evaluation of regression models? *Canadian Journal of Forest Research*, 33, 976–987.
- Lorenzen, B., & Jensen, A. (1989). Changes in leaf spectral properties induced in barley by cereal powdery mildew. *Remote Sensing of Environment*, 27, 201–209.
- Maccioni, A., Agati, G., & Mazzinghi, P. (2001). New vegetation indices for remote measurement of chlorophylls based on leaf directional reflectance spectra. *Journal of Photochemistry and Photobiology, B: Biology*, 61(1–2), 52–61.
- Maloney, K., Boughton, J., & Schneeberger, N. (2006). *Emerald Ash Borer - 2006 Brief*. Newtown Square, PA: USDA Forest Service, Northeastern Area, State and Private Forestry.
- McCullough, D. G., & Katovich, A. S. (2004). *Emerald Ash Borer. Pest Alert*. Newtown Square, PA: USDA Forest Service NA-PR-02-04.
- Mc Murtey III, J. E., Chappelle, E. W., Kim, M. S., Meisinger, J. J., & Corp, L. A. (1994). Distinguish nitrogen fertilization levels in field corns (*Zea mays L.*) with actively induced fluorescence and passive reflectance measurements. *Remote Sensing of Environment*, 47, 36–44.
- Millers, I., Lachance, D., Burkman, W. G., & Allen, D. C. (1991). *North American sugar maple decline project, organization and field methods*. Radnor, PA: Gen. Tech. Rep. NE-154. USDA Forest Service 126 pp.
- Mohammed, G. H., Binder, W. D., & Gillies, S. L. (1995). Chlorophyll fluorescence — a review of its practical forestry applications and instrumentation. *Scandinavian Journal of Forest Research*, 10, 383–410.
- Osborne, B. G., & Fearn, T. (1986). *Near-Infrared spectroscopy in Food Analysis*. New York: John Wiley & Sons Inc.
- Pearson, L., & Miller, L.D. (1972). Remote mapping of standing crop biomass for estimation of the productivity of the short-grass prairie, Pawnee National Grasslands, Colorado. *Proceedings of the 8th International Symposium on Remote Sensing of the Environment* (pp. 1357–1381).
- Penuelas, J., Filella, I., Biel, C., Serrano, L., & Save, R. (1993). The reflectance at the 950–970 nm region as an indicator of plant water status. *International Journal of Remote Sensing*, 14, 1887–1905.
- Penuelas, J., Filella, I., Lloret, P., Munoz, F., & Vilajeliu, M. (1995). Reflectance assessment of mite effects on apple-trees. *International Journal of Remote Sensing*, 16, 2727–2733.
- Penuelas, J., Filella, I., Serrano, L., & Save, R. (1996). Cell wall elasticity and water index (R970 nm R900 nm) in wheat under different nitrogen availabilities. *International Journal of Remote Sensing*, 17, 373–382.
- Penuelas, J., Gamon, J., Freeden, A., Merino, J., & Field, C. (1994). Reflectance indices associated with physiological changes in nitrogen and water limited sunflower leaves. *Remote Sensing of Environment*, 48, 135–146.
- Pontius, J. A., Hallett, R. A., & Martin, M. E. (2005). Assessing hemlock decline using hyperspectral imagery: Signature analysis, indices comparison and algorithm development. *Journal of Applied Spectroscopy*, 59, 836–843.
- Pontius, J. A., Hallett, R. A., & Martin, M. E. (2005). Using AVIRIS to assess hemlock abundance and early decline in the Catskills, New York. *Remote Sensing of Environment*, 97, 163–173.
- Pontius, J. A., Martin, M. E., Plourde, L., & Hallett, R. A. (2005). Using hyperspectral technologies to map hemlock decline: Pre-visual decline assessment for early infestation detection. *Proceedings of the Hemlock Woolly Adelgid Symposium, Asheville, NC* (pp. 73–86).
- Rock, B. N., Hoshizaki, T., & Miller, J. R. (1988). Comparison of in situ and airborne spectral measurements of the blue shift associated with forest decline. *Remote Sensing of Environment*, 24, 109–127.
- Rondeaux, G., Steven, M., & Baret, F. (1996). Optimization of soil-adjusted vegetation indices. *Remote Sensing of Environment*, 55, 95–107.
- Roujean, J. -L., & Breon, F. -M. (1995). Estimating PAR absorbed by vegetation from bidirectional reflectance measurements. *Remote Sensing of Environment*, 51(3), 375–384.
- Sims, D. A., & Gamon, J. A. (2002). Relationships Between Leaf Pigment Content and Spectral Reflectance Across a Wide Range of Species, Leaf Structures and Developmental Stages. *Remote Sensing of Environment*, 81, 337–354.
- Smith, R. C. G., Adams, J., Stephens, D. J., & Hick, P. T. (1995). Forecasting wheat yield in a Mediterranean-type environment from the NOAA satellite. *Australian Journal of Agricultural Research*, 46, 113–125.
- Strasser, R. J., Srivastava, A., & Govindjee (1995). Polyphasic chlorophyll a fluorescence transient in plants and cyanobacteria. *Photochemistry and Photobiology*, 61, 32–42.
- Strasser, R. J., & Tsimilli-Michael, M. (2001). Stress in plants, from daily rhythm to global changes, detected and quantified by the JIP-test. *Chimie Nouvelle. Belgian Royal Society of Chemistry*, 75, 3321–3326.
- Sucharita, G., Innes, J. L., & Hoffmann, C. (1995). Observer variation as a source of error in assessments of crown condition through time. *Forest Science*, 41(2), 235–254.
- Sydnor, T. D., Bumgardner, M., & Todd, A. (2007). The potential economic impacts of emerald ash borer (*Agilus planipennis*) on Ohio, U.S., Communities. *International Society of Arboriculture*, 33(1), 45–54.
- Tucker, C. J. (1979). Red and photographic infrared linear combinations for monitoring vegetation. *Sensing of Environment*, 8, 127–150.

- USDA Forest Service. (1997). *Forest health monitoring 1997 field methods guide*. Research Triangle Park, NC: U.S. Department of Agriculture, Forest Service, National Forest Health Monitoring Program.
- USDA Forest Service. (2004). *Forest inventory and analysis national core field guide*. Vol. 1: Field Data Collection Procedures for Phase 2 Plots, Version 2. Washington, DC.: US Department of Agriculture, Forest Service, Washington Office.
- Vogelmann, J. E., & Rock, B. N. (1988). Assessing forest damage in high-elevation coniferous forests in Vermont and New-Hampshire using Thematic Mapper data. *Remote Sensing of Environment*, 24, 227–246.
- Vogelmann, J. E., Rock, B. N., & Moss, D. M. (1993). Red edge spectral measurements from sugar maple leaves. *International Journal of Remote Sensing*, 14, 1563–1575.
- Williams, P., & Norris, K. (2001). *Near-Infrared Technology in the Agricultural and Food Industries*. St. Paul, MN: American Association of Cereal Chemists, Inc.
- Zarco-Tejada, P.J. (2000). Dissertation: Hyperspectral remote sensing of closed forest canopies: Estimation of chlorophyll fluorescence and pigment content. Toronto, Ontario, Canada: York University.
- Zarco-Tejada, P. J., Berjon, A., Lopez-Lozano, R., Miller, J. R., Martin, P., Cachorro, V., Gonzalez, M. R., & de Frutos, A. (2005). Assessing vineyard condition with hyperspectral indices: Leaf and canopy reflectance simulation in a row-structured discontinuous canopy. *Remote Sensing of Environment*, 99, 271–287.
- Zarco-Tejada, P. J., Miller, J. R., Mohammed, G. H., & Noland, T. L. (2000). Chlorophyll fluorescence effects on vegetation apparent reflectance: I. Leaf-level measurements and model simulation. *Remote Sensing of Environment*, 74, 582–595.
- Zarco-Tejada, P. J., Miller, J. R., Mohammed, G. H., Noland, T. L., & Sampson, P. H. (2000). Optical indices as bioindicators of forest condition from hyperspectral CASI data. *Symposium of the European Association of Remote Sensing Laboratories, Valladolid Spain* (pp. 517–522).
- Zarco-Tejada, P. J., Miller, J. R., Mohammed, G. H., Noland, T. L., & Sampson, P. H. (2000). Chlorophyll fluorescence effects on vegetation apparent reflectance: II. Laboratory and airborne canopy-level measurements with hyperspectral data. *Remote Sensing of Environment*, 74, 596–608.
- Zarco-Tejada, P. J., Miller, J. R., Noland, T. L., Mohammed, G. H., & Sampson, P. H. (2001). Scaling-up and model inversion methods with narrowband optical indices for chlorophyll content estimation in closed forest canopies with hyperspectral data. *IEEE Transactions on Geoscience and Remote Sensing*, 39, 1491–1507.